An Autozeroing Floating-Gate Amplifier

Paul Hasler, *Member, IEEE*, Bradley A. Minch, *Member, IEEE*, and Chris Diorio, *Member, IEEE*

***Abstract*—We have developed a bandpass floating-gate amplifier that uses tunneling and pFET hot-electron injection to set its dc operating point adaptively. Because the hot-electron injection is an inherent part of the pFET's behavior, we obtain this adaptation with no additional circuitry. Because the gate currents are small, the circuit exhibits a high-pass characteristic with a cutoff frequency less than 1 Hz. The high-frequency cutoff is controlled electronically, as is done in continuous-time filters. We have derived analytical models that completely characterize the amplifier and that are in good agreement with experimental data for a wide range of operating conditions and input waveforms. This autozeroing floating-gate amplifier demonstrates how to use continuous-time floating-gate adaptation in amplifier design.**

***Index Terms*—AFGA, capacitive circuits, electron tunneling, floating-gate circuits, hot-electron injection.**

I. Introduction

WE PRESENT a bandpass floating-gate amplifier that uses tunneling and pFET hot-electron injection so that it can return to its sensitive region despite large changes in the dc input voltage. Offsets often present a difficult problem for designers of MOS analog circuits. A time-honored tradition for addressing this problem is to use a blocking capacitor to eliminate the input dc component. However, for integrated filters, this approach requires enormous input capacitors and resistors to get time constants of less than 1 Hz. Existing on-chip autozeroing techniques rely on clocking schemes that compute the input offset periodically, then subtract the correction from the input [1]. These autozeroing techniques add significant complexity to the circuit, as well as to clock noise, aliasing, etc.

We previously introduced the *autozeroing floating-gate amplifier* (AFGA) [2], [3]; here, we present the circuit analysis and the experimental data in much greater detail. The AFGA is an integrated continuous-time filter that is intrinsically autozeroing. It can achieve a high-pass characteristic at frequencies well below 1 Hz. In contrast with conventional autozeroing amplifiers that eliminate their input offset, the AFGA nulls its output offset. The AFGA is a continuous-time filter; it does not require any clocking. Our AFGA is the first known application of pFET hot-electron injection. Until now, pFET hot-electron injection has attracted attention only as a source of MOSFET oxide degradation [4]; therefore, this circuit presents an interesting case of turning a bug into a feature. The autozeroing technique used in the AFGA can be applied to a wide variety of floating-gate MOS circuits, such as those presented by us elsewhere [5], to continuously restore a desired baseline operation on a slow timescale.

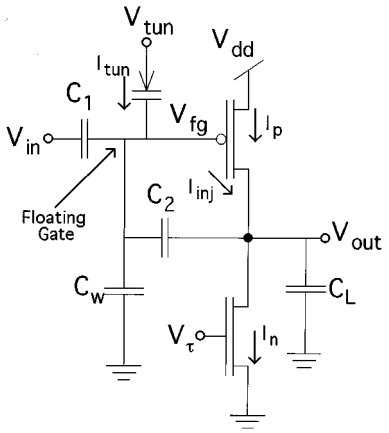

Fig. 1. An AFGA that uses pFET hot-electron injection. The ratio of C_2 to C_1 sets the gain of this inverting amplifier. The nFET is a current source and sets the current through the pFET. Steady state occurs when the injection current is equal to the tunneling current. The capacitance from the floating gate to ground C_w represents both the parasitic and the explicitly drawn capacitances. Increasing C_w will increase the linear input range of the circuit. The capacitance connected to the output terminal C_L is the load capacitance. Between $V_{\rm tun}$ and $V_{\rm fg}$ is our symbol for a tunneling junction, which is a capacitor between the floating-gate and an n-well.

In Section II, we give a qualitative overview of AFGA operation. In Section III, we present a circuit-level model of electron tunneling and of pFET hot-electron injection. In Section IV, we consider the AFGA's high-pass filter behavior; we also address long-term parameter drift. In Section V, we consider the AFGA's low-pass filter behavior. In Section VI, we describe the AFGA's frequency response and dynamic range. We conclude in Section VII. We discuss other AFGA effects elsewhere, including change in equilibrium voltages of the AFGA due to changes in biasing, tunneling voltages, and large input amplitude [3]. Further, we will concentrate on subthreshold biasing of the AFGA; an AFGA biased with above-threshold currents shows qualitatively similar behavior, but the quantitative behavior is different [3].

II. Qualitative AFGA Operation

Fig. 1 shows the autozeroing floating-gate amplifier. The open-loop amplifier consists of a pFET input transistor and an nFET current source. With capacitive feedback, the input signal is amplified by a closed-loop gain approximately equal to $-(C_1/C_2)$. The maximum gain is limited both by the open-loop gain and by the parasitic floating-gate-to-drain overlap capacitance.

Manuscript received April 2000; revised November 2000. This work was supported by Center for Neuromorphic Systems Engineering as a part of the NSF ERC Program. This paper was recommended by Associate Editor T. S. Lande.

P. Hasler is with the School of Electrical and Computer Engineering, Georgia Institute of Technology, Atlanta, GA 30332-0250 USA (e-mail: phasler@ee.gatech.edu).

B. A. Minch is with the Department of Electrical Engineering, Cornell University, Ithaca, NY 14853 USA (e-mail: minch@ee.cornell.edu).

C. Diorio is with the Department of Computer Science, University of Washington, Seattle, WA 98195 USA (e-mail: diorio@cs.washington.edu).

Publisher Item Identifier S 1057-7130(01)02019-5.

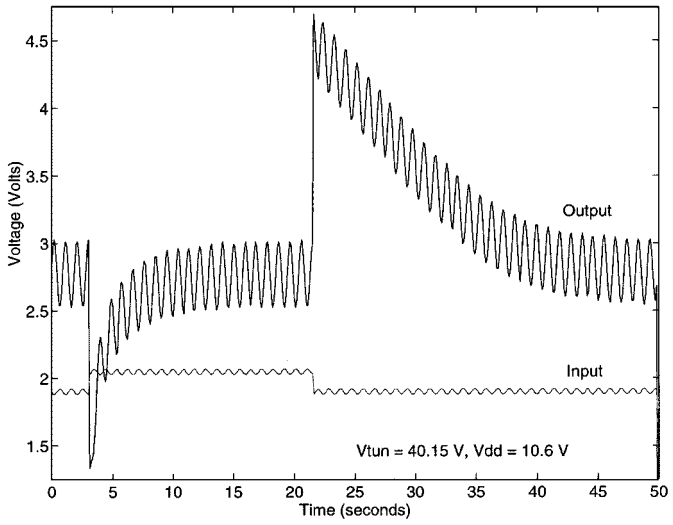

Fig. 2. Response of the AFGA to a 1-Hz sinewave superimposed on a 19-s voltage pulse. The AFGA has a closed-loop gain of 11.2 and a low-frequency cutoff at 100 mHz. We see that the signal is amplified, but the much slower step is adapted away.

The complementary tunneling and hot-electron injection processes adjust the floating-gate charge such that the amplifier's output voltage returns to a steady-state value on a slow timescale. If the output voltage is below its equilibrium value, then the injection current exceeds the tunneling current, decreasing the charge on the floating gate; that, in turn, increases the output voltage back toward its equilibrium value. If the output voltage is above its equilibrium value, then the tunneling current exceeds the injection current, increasing the charge on the floating gate; that, in turn, decreases the output voltage back toward its equilibrium value. Because this circuit returns the output voltage to the same equilibrium value on a slow timescale, this circuit behaves like a high-pass filter with a long time constant.

Two conditions must be satisfied for the circuit to be in equilibrium. First, the pFET channel current I_p must be equal to the nFET channel current I_n. We define this quiescent channel current as I_{s0}. Second, the injection gate current must be equal to the tunneling gate current. We define I_{inj0} as the quiescent injection current that must equal I_{tun0}, the quiescent tunneling current, at equilibrium. Since the tunneling and injection currents are many orders of magnitude smaller than I_{so} and are charging similar-sized capacitances, the first condition is satisfied much faster than is the second condition. The frequency range over which the first condition is satisfied, but the second condition is not satisfied, is where the AFGA behaves as an amplifier. The combination of electron tunneling and pFET hot-electron injection applies the appropriate negative feedback to stabilize the output voltage such that the second condition also is satisfied.

In the frequency range where the first condition does not hold, the output voltage is attenuated. In this regime, the circuit behaves as a low-pass filter. Since the output capacitances are charged or discharged by currents on the scale of I_{s0}, the cutoff frequency will be directly dependent on the bias current. Continuous-time integrators operate on a similar principle [6], [7]. The AFGA transfer function is bandpass, with the low-frequency cutoff set by the equilibrium tunneling and injection currents and the high-pass cutoff independently set by the equilibrium pFET and nFET channel currents.

Fig. 2 shows the response of the autozeroing floating-gate amplifier to a 1-Hz sine wave superimposed on an input pulse. If the input changes on a timescale that is much shorter than the adaptation, then the output is an amplified version of the input signal. The amplifier adapts to the pulse input after an initial transient while preserving the amplified 1-Hz sine wave.

We present data from an AFGA fabricated in the 2-μm n-well CMOS process available through MOSIS. Typical operating values for V_{tun} were between 33 and 42 V; those for V_{dd} were between 6 and 12 V. We obtained similar data in a 1.2-μm n-well CMOS process available through MOSIS, but with typical operating values for V_{tun} between 26 V and 31 V; and in the 0.5-; μm n-well process available through MOSIS, but with typical operating values for V_{tun} at 12 V and V_{dd} at 5 V. For more modern processes, the typical operating voltages will decrease because of thinner gate oxides and higher dopant impurity concentrations.

III. Circuit Model of a pFET with Hot-Electron Injection and Electron Tunneling

Before we consider the behavior of the autozeroing amplifier, we review electron tunneling and pFET hot-electron injection. We begin with the basic subthreshold MOS characteristics [7], which are valid even at large drain-to-source voltages. For subthreshold operation, we can describe the nFET and pFET channel current for a change in gate voltage ΔV_g around a bias current I_{so} as

$$\begin{aligned} \text{nFET: } I_n &= I_{\mathrm{so}} e^{\kappa_n \Delta V_g / U_T} e^{\Delta V_d / V_A} \\ \text{pFET: } I_p &= I_{\mathrm{so}} e^{-\kappa \Delta V_g / U_T} e^{-\Delta V_d / V_A} \end{aligned} \tag{1}$$

where κ_n, κ is the fractional change in the nFET, pFET surface potential due to a change in ΔV_g, respectively; V_A is the Early voltage of the nFET or pFET; and U_T is the thermal voltage kT/q. The Early voltage is directly related to the amplifier's open-loop gain; for this amplifier, the maximum open-loop gain is roughly 700. The Early voltage decreases at large drain-to-source voltages due to impact ionization in the drain-to-channel depletion region [3]. In the drain-to-channel depletion region, holes are accelerated to large energies; if a hole has an energy larger than the bandgap, then it may undergo impact ionization. The result of an impact ionization is two holes and one electron. For the nFET biased with a drain-to-source voltage of 3.0 V and the pFET biased with a drain-to-source voltage of 8.5 V, V_o is nearly constant for both transistors [3]; therefore the AFGA's open-loop gain also is nearly constant.

Next, we consider the model of electron tunneling and hot-electron injection. As we showed in [9] and [8], we approximate the tunneling current for a fixed bias on the tunneling line by

$$I_{\mathrm{tun}} = I_{\mathrm{tun0}} e^{(\Delta V_{\mathrm{tun}} - \Delta V_{\mathrm{fg}})/V_x} \tag{2}$$

where

- V_x parameter related to the quiescent tunneling and floating-gate voltages;
- $\Delta V_{\rm tun}$ change in the tunnneling voltage;
- $\Delta V_{\rm fg}$ change in the floating-gate voltage from the quiescent floating-gate voltage.

For our operating conditions, a typical value of V_x is 1 V with the 42-nm oxide used in the 2.0-μm Orbit process. As we showed in [8], we approximate the hot-electron injection current by

$$I_{\rm inj} = I_{\rm inj0}\left(\frac{I_p}{I_{s0}}\right)^{\alpha}\exp\left(\frac{-\Delta V_d}{V_{\rm inj}}\right) = I_{\rm inj0}\exp\left(-\frac{\alpha\kappa\Delta V_{\rm fg}}{U_T}-\frac{\Delta V_d}{V_{\rm inj}}\right) \tag{3}$$

where

- I_{s0} quiescent source current;
- V_d drain voltage;
- $V_{\rm inj}$ measurable device parameter;
- α $1-(U_T/V_{\rm inj})$.

For a quiescent $\Phi_{\rm dc} = 8.2$ V, a typical value for $V_{\rm inj}$ is 250 mV. A typical value of α is 0.90, which is consistent with $V_{\rm inj}$ equal to 250 mV.

IV. Low-Frequency AFGA Behavior

We can write two general equations governing the AFGA behavior around an equilibrium output voltage. We obtain the first equation by applying Kirchoff's current law (KCL) at the floating gate

$$(C_1+C_2+C_w)\frac{dV_{\rm fg}}{dt} = C_1\frac{dV_{\rm in}}{dt}+C_2\frac{dV_{\rm out}}{dt} + I_{\rm tun0}\left(1-\exp\left(-\alpha\frac{\kappa\Delta V_{\rm fg}}{U_T}-\frac{\Delta V_{\rm out}}{V_{\rm inj}}\right)\right). \tag{4}$$

We obtain the second equation by applying KCL at the output node

$$(C_2+C_L)\frac{dV_{\rm out}}{dt} = C_2\frac{dV_{\rm fg}}{dt}+I_\tau\left(e^{-\kappa\Delta V_{\rm fg}/U_T}-1\right). \tag{5}$$

We have neglected the Early effect, which adds a correction term to (5). As long as the closed-loop gain is much lower than the amplifier gain, ignoring the Early effect is a good approximation.

In the passband, where the AFGA is an amplifier, the floating gate is held nearly fixed by the amplifier feedback, and the tunneling and injection currents are negligible. This approximation simplifies (4) to

$$C_2\frac{dV_{\rm out}}{dt} = -C_1\frac{dV_{\rm in}}{dt}. \tag{6}$$

Thus, the change in the output voltage ($\Delta V_{\rm out}$) is equal to the input voltage ($\Delta V_{\rm in}$) amplified by $-(C_1/C_2)$.

A. Low-Frequency Model

We make two approximations to model the low-frequency response of the AFGA. First, the open-loop gain from the floating gate to the output can be large; a typical value is 700. If we are to keep the output voltage between the supply rails, the floating-gate voltage must be confined to a 10-mV swing. Thus, we approximate the floating-gate voltage to be constant. Second, because the floating-gate voltage is nearly constant, the source current varies only slightly. The quiescent source current (I_{s0}) is set by the nFET current source. From (2) and (3), the model of injection current for a fixed source current I_{s0} is

$$I_{\rm tun}-I_{\rm inj} = I_{\rm tun0}\left(1-\exp\left(-\frac{\Delta V_{\rm out}}{V_{\rm inj}}\right)\right) \tag{7}$$

where $I_{\rm tun0} = I_{\rm inj0}$ for the circuit in equilibrium. Since the floating gate is held nearly constant by feedback, the floating-gate voltage dependence in (3) is negligible. Even when the circuit is biased with above-threshold currents, the tunneling current still is nearly fixed. Since the injection efficiency is still an exponential function of the drain voltage for above-threshold currents, the low-frequency dynamics are similar in below- and above-threshold operation.

With the preceding approximations, we can model the amplifier's output voltage $V_{\rm out}$ in terms of $V_{\rm in}$ with a single equation. The total floating-gate current is the sum of the capacitive currents of the input and output terminals, plus the tunneling and injection currents. From (4), we write

$$C_2\frac{dV_{\rm out}}{dt} = -C_1\frac{dV_{\rm in}}{dt}+I_{\rm tun0}\left(\exp\left(-\frac{\Delta V_{\rm out}}{V_{\rm inj}}\right)-1\right). \tag{8}$$

To solve (8), we make the following change of variables: $X = e^{\Delta V_{\rm out}/V_{\rm inj}}$. The resulting equation for X is a linear first-order differential equation with variable coefficients

$$\tau_l\frac{dX}{dt} = \frac{\tau_l A_v X}{V_{\rm inj}}\frac{dV_{\rm in}}{dt}+1-X \tag{9}$$

where τ_l, the low-frequency cutoff, is equal to $C_2V_{\rm inj}/I_{\rm tun0}$ and A_v is the closed-loop ac gain of the amplifier $-(C_1/C_2)$.

B. Response to a Voltage Step

Consider the AFGA's response to an input voltage step. Assume that the output voltage has adapted initially to its steady-state value. To solve (9), we first assume that the output voltage immediately after applying the step $\Delta V_{\rm out}(0^+)$ is given by the magnitude of the input step times the AFGA ac gain. We employ $\Delta V_{\rm out}(0^+)$ as a new, effective initial condition and denote the effective initial condition in X by $X(0^+) = e^{V_{\rm out}(0^+)/V_{\rm inj}}$. For a downward step, $X(0^+)$ is greater than one; for an upward step, $X(0^+)$ is less than one. After the input step, $dV_{\rm in}/dt = 0$; therefore, (9) becomes

$$\begin{cases}\tau_l\dfrac{dX}{dt} = 1-X\\ X(0) = X(0^+).\end{cases} \tag{10}$$

The solution to (10) in terms of $\Delta V_{\rm out}$ is

$$\Delta V_{\rm out}(t) = V_{\rm inj}\ln\left(1+(X(0^+)-1)e^{-t/\tau_l}\right) \tag{11}$$

where $\Delta V_{\rm out}\to 0$ as $t\to\infty$.

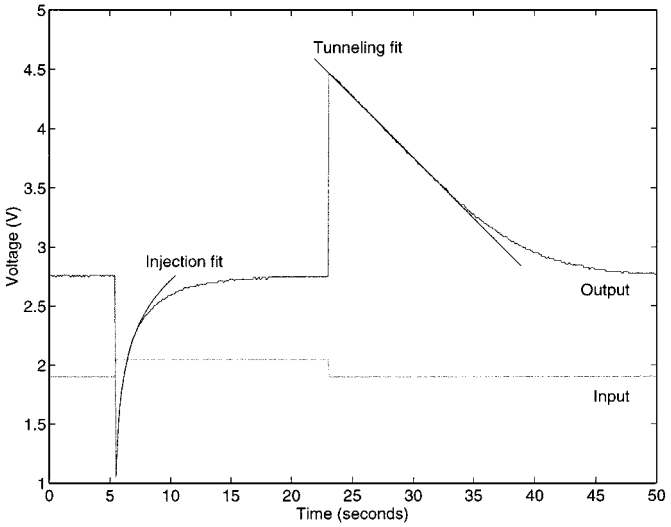

Fig. 3. Response of the AFGA to an upgoing and downgoing step input. The adaptation in response to an upward step results from electron tunneling; the adaptation in response to a downward step results from pFET hot-electron injection. This amplifier had a gain of 11.2. We plot the curve fits of the simplified expressions of, where either tunneling or injection dominates the restoration process. From the fits, τ is 4.3 s and $I_{\rm tun0}$ is 50 fA. The value of τ can be set reliably to more than 10^5 s. The steady-state output voltage decreased for increasing tunneling voltages.

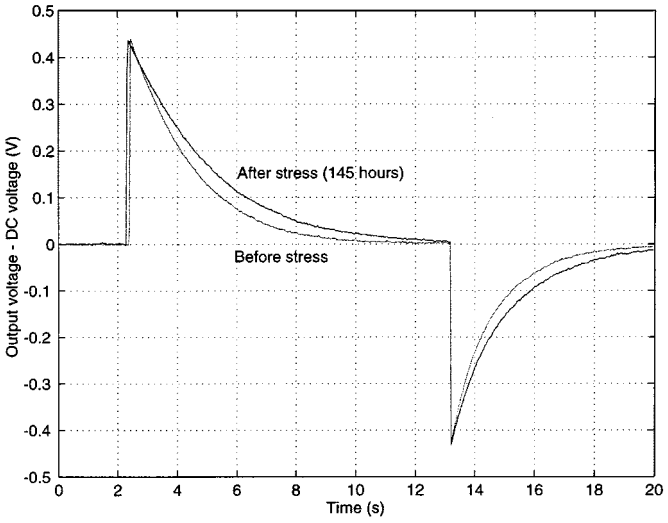

Fig. 4. The effect of long-duration AFGA operation by showing the step responses to an upgoing and downgoing voltage step before and after 145 h of operation. We plot the difference in the output voltage from the equilibrium dc level as a function of time; the equilibrium output voltage increased slightly over the 145 h of operation. By extracting the device parameters as a function of time, we see that the long-term change is due primarily to long-term change from tunneling junction [3].

The step response has three interesting regimes, which are approximated by

$$\Delta V_{\rm out} \approx \begin{cases} \Delta V_{\rm out}(0^+)e^{-(t/\tau_l)}, & X(0^+) \approx 1 \\ \Delta V_{\rm out}(0^+) - \dfrac{I_{\rm tun0}}{C_2}\,t, & X(0^+) \gg 1 \\ V_{\rm inj}\,\ln\left(X(0^+) + \dfrac{t}{\tau_l}\right), & X(0^+) \ll 1. \end{cases} \tag{12}$$

The first case occurs when the tunneling current is nearly equal to the injection current just after the voltage step. The solution in this region is the familiar exponential decay of a linear system. The second case occurs when the tunneling current dominates the injection current. The behavior of the output voltage in this regime results from the constant tunneling current's removing electrons from the floating gate. The third case occurs when the injection current dominates the tunneling current. Fig. 3 shows a measured response to an input pulse, with curve fits to the regions where either the tunneling or injection current dominates.

C. Long-Term Parameter Drift

The physical properties of the tunneling and hot-electron injection mechanisms change with time. These processes are permanently modified as electrons pass through the oxide, creating electron traps. We investigated the long-term changes by performing an accelerated stress experiment, where we operated an AFGA continuously for 145 h with an average τ_l of 1.7 s. When an AFGA is used as an amplifier or as a low-pass filter, a more reasonable τ_l would be at least several minutes; therefore, this experiment is equivalent to the stress of operating the AFGA continuously for a few years, because trap creation is proportional to the total charge traveling through the oxide. The effect of an input signal only slightly modifies the results of this experiment. To characterize the behavior of the AFGA over time, we performed a square-wave experiment, similar to the one shown in Fig. 3, once per hour for 145 h. To each of the resulting output waveforms, we fit the expressions of (12) and extracted the relevant device parameters. Fig. 4 shows the square-wave response of the AFGA before and after this lifetime test. The adaptation time constant has increased noticeably, but the general behavior is unaffected. By extracting the device parameters as a function of time, we see that the long-term change is due primarily to long-term change from the tunneling junction [3].

V. High-Frequency AFGA Behavior

For sufficiently high frequencies, the autozeroing floating-gate amplifier is a low-pass filter. In this regime, the tunneling and injection currents are negligible; therefore, we approximate (4) as

$$C_T\,\frac{dV_{\rm fg}}{dt} = C_1\,\frac{dV_{\rm in}}{dt} + C_2\,\frac{dV_{\rm out}}{dt} \tag{13}$$

where we define $C_T = C_1 + C_2 + C_w$. From (13), we see that changes in $V_{\rm out}$ are proportional to changes in $V_{\rm fg}$ and $V_{\rm in}$. At extremely high frequencies, the transistor channel currents are negligible compared to the capacitive currents. In this capacitive-feedthrough regime, the solutions to (5) and (13) are

$$\frac{\Delta V_{\rm fg}}{\Delta V_{\rm in}} = \frac{C_1 C_o}{C_T C_o - C_2^2}, \quad \frac{\Delta V_{\rm out}}{\Delta V_{\rm in}} = \frac{C_1 C_2}{C_T C_o - C_2^2} \tag{14}$$

where we define $C_o = C_L + C_2$. We can reduce the effects of the capacitive feedthrough by increasing either C_L or C_W.

At frequencies between the low-frequency cutoff and the capacitive-feedthrough regime, the behavior of the AFGA results from the floating-gate voltage's settling back to its equilibrium

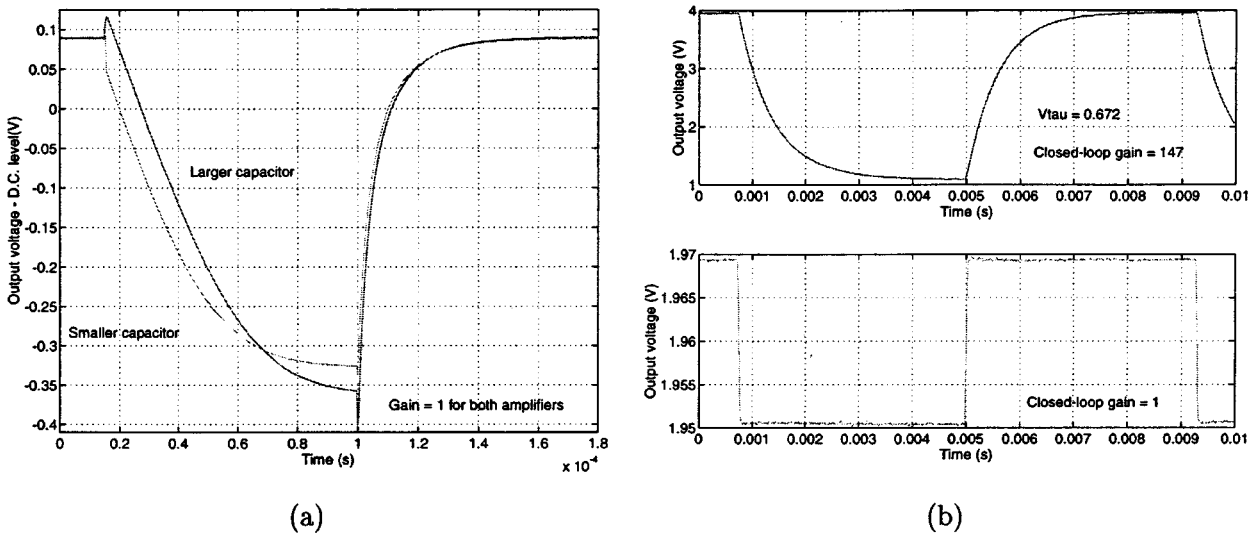

Fig. 5. High-frequency AFGA behavior. (a) Two AFGAs with unity gain but with different values for C_1. The larger capacitor circuit had $C_1 = C_2 = 300$ fF, whereas the smaller-capacitor circuit had $C_1 = C_2 = 50$ fF. For both AFGAs, C_L was the same. We operated the two AFGAs with different subthreshold bias currents to achieve comparable settling times. (b) Two AFGAs with different gains.

value. Therefore, we combine (5) and (13) to form a single equation for the floating-gate voltage, which we write as

$$\left(\frac{C_T C_o - C_2^2}{C_2 I_\tau}\right)\frac{dV_{\rm fg}}{dt} = \frac{C_1 C_o}{C_2 I_\tau}\frac{dV_{\rm in}}{dt} + e^{-\kappa \Delta V_{\rm fg}/U_T} - 1. \tag{15}$$

This equation is similar to (9), which describes the output-voltage response in the low-frequency case. As we did in that case, substituting $Y = e^{\kappa \Delta V_{\rm fg}/U_T}$ into (15) results in the linear differential equation

$$\tau_h \frac{dY}{dt} = \frac{\tau_{h2}\kappa}{U_T}\frac{dV_{\rm in}}{dt}Y + 1 - Y \tag{16}$$

where we define τ_{h2} to be $\tau_{h2} = C_1 C_o U_T/\kappa C_2 I_\tau$, which is the time constant that marks the onset of capacitive feedthrough. We define τ_h to be

$$\tau_h = \frac{(C_T C_o - C_2^2)U_T}{\kappa C_2 I_\tau} \tag{17}$$

which represents the high-frequency cutoff.

As we did in the low-frequency case, we shall consider the response to an input voltage step. To solve (16), we first assume that the floating-gate voltage immediately after applying the step $\Delta V_{\rm fg}(0^+)$ is given by the magnitude of the input step attenuated by the capacitive divider ratio [(14)]. With this initial condition, the solution is

$$\Delta V_{\rm fg} = \frac{U_T}{\kappa}\ln\left(1 + \left(e^{\kappa \Delta V_{\rm fg}(0^+)/U_T} - 1\right)e^{-t/\tau_h}\right). \tag{18}$$

After the initial jump, given by (14), the output voltage is related to the floating-gate voltage by $\Delta V_{\rm out} = (C_T/C_2)\Delta V_{\rm fg}$.

Fig. 5 shows measured AFGA output-voltage responses to several square-wave inputs. Fig. 5(a) shows the responses of two unity-gain AFGAs with different capacitor values to the same square-wave input. As in the low-frequency case, the high-frequency response of the AFGA is asymmetric: the downgoing step response approaches its steady state linearly with time, and the upgoing step response approaches its steady state logarithmically with time. The initial jump in the downgoing step is due to capacitive feedthrough. From these data, it is evident that decreasing C_1 and C_2 without changing C_L will decrease the amount of capacitive feedthrough. Fig. 5(b) shows the voltage responses to a small input step for two AFGAs with gains of 1 and 146. The response from the unity-gain AFGA is a buffered version of the input; the high-gain AFGA shows a linear first-order low-pass filtered version of the input. These responses illustrate the gain-bandwidth tradeoff in the AFGA.

The linear 3-V output swing in the high-gain response of Fig. 5(b) raises this question: What determines the linear range of an AFGA? Our criterion for linearity is that $\Delta V_{\rm fg}$ be sufficiently small that the factor $(\exp(-(\kappa \Delta V_{\rm fg}/U_T)) - 1)$ in (15) can be approximated by $-(\kappa \Delta V_{\rm fg}/U_T)$. This criterion implies that the floating-gate voltage must not move by more that U_T/κ from its equilibrium value. The floating-gate voltage has its maximum swing in the capacitive-feedthrough regime; therefore, from (14), the input linear range $V_{\rm Li}$ is $V_{\rm Li} = U_T/\kappa(C_T/C_1)B$, where we define $B = 1 - (C_2^2/C_T C_o)$. For amplifiers with gains greater than or equal to one, which requires that C_1 be greater than C_2, B is bounded between one-half and one for all C_1, C_2, C_W, and C_L. Further, if the AFGA is driving a C_L that is at least as big as C_1, B is bounded between three-quarters and one. Consequently, B can be considered a correction term.

We express the output linear range $V_{\rm Lo}$ in terms of the input linear range $V_{\rm Li}$ by $V_{\rm Lo} = (U_T/\kappa)(C_T/C_2)B$, which is $V_{\rm Li}$ times the amplifier gain C_1/C_2. The output linear range scales with the amplifier gain. By increasing C_w, we can reduce the change in the floating-gate voltage, thereby increasing the amplifier's output linear range. The AFGA's gain from input to output in the passband is

$$\frac{V_{\rm out}}{V_{\rm in}} = -\frac{C_1}{C_2}\frac{1}{1 + \dfrac{C_1 + C_2 + C_W}{C_2 A}} = -\frac{C_1}{C_2}\frac{1}{1 + \dfrac{\kappa V_{\rm Lo}}{A U_T B}} \tag{19}$$

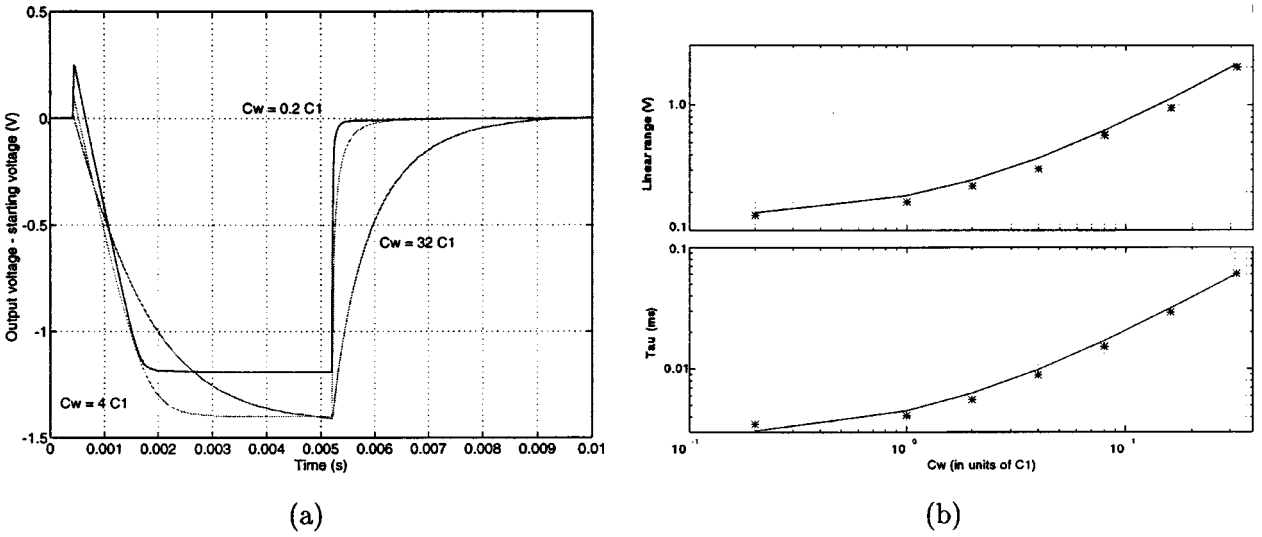

Fig. 6. Linear range of the AFGA versus C_w. (a) The response of three AFGAs to the same square-wave input. All three AFGAs were identical except for their values of C_w and were biased by the same V_τ. Increasing C_w increases the linear range, decreases the amount of capacitive feedthrough, and decreases the low-pass cutoff frequency. (b) Measured linear range and τ_h for several unity-gain AFGAs for different C_w ratioed in units of C_1. The linear range fit is $V_{\rm Li} = 0.063$ V $C_w/C_1 + 0.125$ V, and the τ fit is $\tau = 1.8\ \mu$s $C_w/C_1 + 2.7\ \mu$s.

where A is the gain from floating gate to output. For a sufficiently large A, the AFGA's passband gain is independent of C_w.

Fig. 6 shows measured data demonstrating how τ_h and linear range scale with C_w for unity-gain AFGAs. For a unity-gain AFGA—that is, for $C_1 = C_2$—the expressions for τ_h and input linear range are

$$\tau_h = \frac{U_T(C_1 + C_L)}{\kappa I_\tau}\left(2 - \frac{C_1}{C_1 + C_L} + \frac{C_w}{C_1}\right) \tag{20}$$

and

$$V_{\rm Li} = \frac{U_T}{\kappa}\left(2 - \frac{C_1}{C_1 + C_L} + \frac{C_w}{C_1}\right). \tag{21}$$

The data in Fig. 6 were taken with AFGAs that had no explicitly drawn C_L; the variation between the data and the linear curve fit probably is due to the different parasitic load capacitances. Both from experimental data and from the direct analytic solution of (16), second-harmonic distortion dominates for the AFGAs; for a sine-wave input with amplitude of $V_{\rm Li}$, the peak second harmonic distortion is 0.05% of, or 26 dB below, the fundamental frequency response. The second harmonic distortion is maximum for frequencies just below $1/2\pi\tau_h$; for amplitudes at or below V_L, the second harmonic distortion is proportional to the square of the fundamental amplitude.

VI. Frequency Response of the AFGA

To derive the AFGA frequency response, we begin with the small-signal form of (4) and (5)

$$\begin{aligned} C_T\frac{dV_{\rm fg}}{dt} &= C_1\frac{dV_{\rm in}}{dt} + C_2\frac{dV_{\rm out}}{dt} + \frac{I_{\rm tun0}}{V_{\rm inj}}\Delta V_{\rm out} \\ C_o\frac{dV_{\rm out}}{dt} &= C_2\frac{dV_{\rm fg}}{dt} - \frac{\kappa I_\tau}{U_T}\Delta V_{\rm fg}. \end{aligned} \tag{22}$$

That is, we assume that the input signal is sufficiently small that we need to keep only the linear terms when we expand the exponentials. A small-signal input changes $V_{\rm out}$ by less than $V_{\rm inj}$, due to the injection nonlinearity in the low-frequency regime, and changes $V_{\rm fg}$ by less than U_T/κ, due to the transistor nonlinearity in the high-frequency regime. We shall discuss the response in the low- and high-frequency regimes. Then, we shall present the general solution.

For low-frequency inputs, we can approximate (22) as

$$\tau_l\frac{C_1}{C_2}\frac{dV_{\rm in}}{dt} + \tau_l\frac{dV_{\rm out}}{dt} = -\Delta V_{\rm out} \tag{23}$$

for which the resulting frequency response is

$$\frac{V_{\rm out}(s)}{V_{\rm in}(s)} = -\frac{C_1}{C_2}\frac{s\tau_l}{1 + s\tau_l}. \tag{24}$$

Fig. 7 shows the measured AFGA frequency response: for the high-gain AFGA, τ_l is 20 mHz; for the low-gain AFGA, τ_l is 300 μHz. The high-gain AFGA has a gain of 146; the low-gain AFGA has unity gain.

For high-frequency inputs, we can simplify (22) by assuming input frequencies much larger than $1/2\pi\tau_l$; we write the result as

$$\frac{V_{\rm out}}{V_{\rm in}} = -\frac{C_1}{C_2}\frac{1 - \tau_{h2}s}{1 + \tau_h s}. \tag{25}$$

This transfer function includes the effects of parasitic and load capacitances. The response in (25) is the transfer function of a first-order system; because we use capacitive feedback, the AFGA is stable for any value of closed-loop gain. As we can see in Fig. 7, $1/2\pi\tau_h$ is 500 Hz for the high-gain AFGA and is 40 kHz for the low-gain AFGA.

We obtain the response for all frequencies by taking the Laplace transform of (22), and solve to obtain

$$\frac{V_{\rm out}(s)}{V_{\rm in}(s)} = -\frac{C_1}{C_2}\frac{1 - \tau_{h2}s}{1 + \tau_h s + \dfrac{1}{\tau_l s}} \tag{26}$$

where τ_l, τ_h, τ_{h2} are as defined previously.

When we consider the frequency response of the AFGA, it is natural to consider the output-voltage spectrum for no

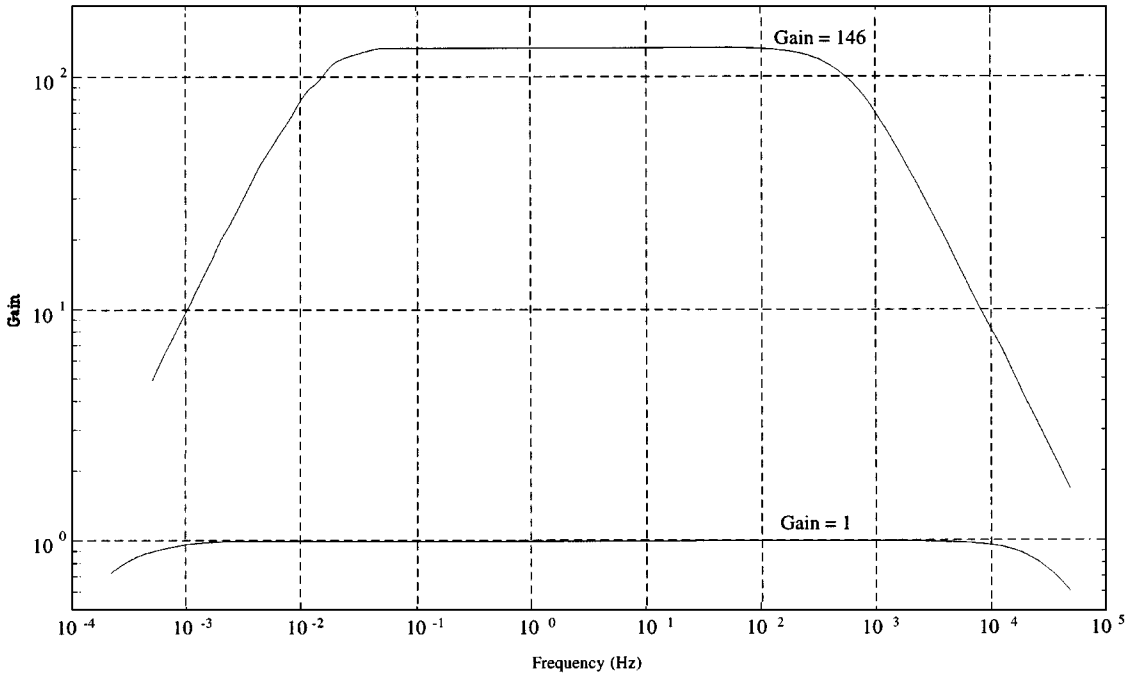

Fig. 7. Frequency response for two AFGAs with different gains. For both the high- and low-gain AFGA, $C_1 + C_2$ is approximately constant. For the high-gain AFGA, τ_l is 20 mHz and τ_h is 600 Hz; for the low-gain AFGA, τ_l is 300 μHz and τ_h is 40 kHz. The ratio of τ_h and τ_l between the two AFGAs are equal to one-half of the ratio of the gains; the ratio is consistent with a constant $C_1 + C_2$.

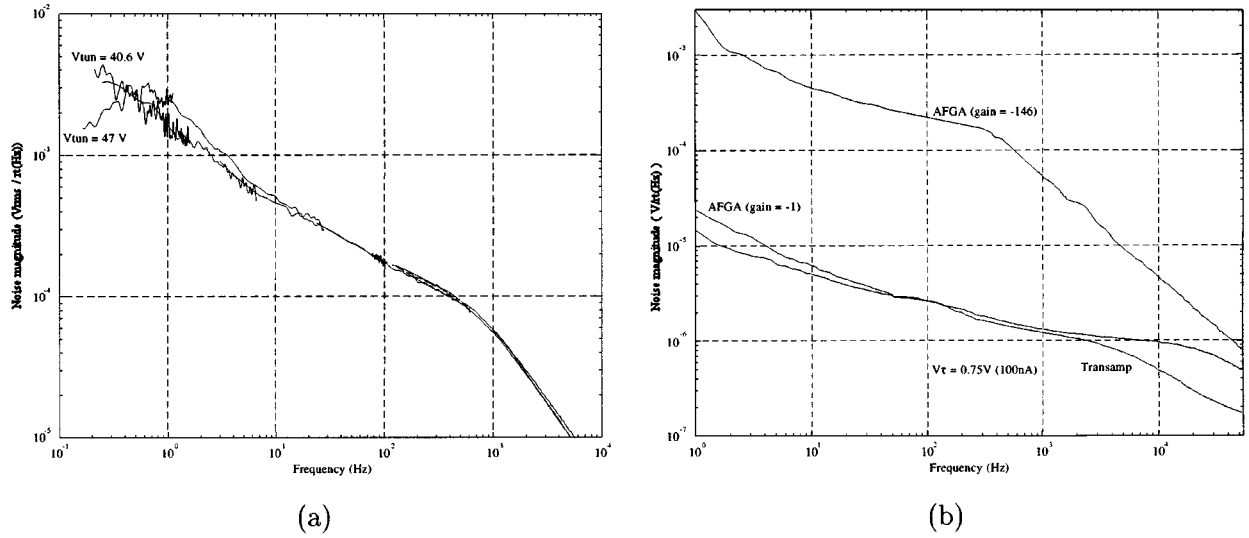

Fig. 8. Noise spectrum of an AFGA for a constant input. (a) Output noise spectrum of an AFGA with a gain of 146 for two different tunneling voltages ($V_{\rm tun}$). The low-frequency cutoff eliminates $1/f$ noise at frequencies below $1/2\pi\tau_l$. The spectrum was taken for a bias current of 80 nA, which corresponds to a V_τ of 0.73 V. (b) Comparison of a high-gain AFGA with a unity-gain AFGA and with a generic follower-connected differential amplifier. All three amplifiers had the same V_τ voltage and the same bias current. The sums of C_1 and C_2 are the same for the two AFGAs.

input—that is, the output-voltage noise from the amplifier. Fig. 8 shows AFGA output-voltage spectra for a fixed voltage-source input. We see that for low frequencies, $1/f$ noise is dominant; for high frequencies, thermal noise dominates. The AFGA attenuates the $1/f$ noise below the low-frequency cutoff. Fig. 8(a) shows that we can reduce the $1/f$ noise by increasing $V_{\rm tun}$, and thereby decreasing τ_l. Fig. 8(b) shows a comparison among a high-gain AFGA, a unity-gain AFGA, and a follower-connected transconductance amplifier. The transconductance amplifier is the wide-range amplifier described previously [7]; it has transistors larger than those of the AFGAs, resulting in the lower $1/f$ noise. The AFGAs used a constant tunneling current; because the noise spectrum of the unity-gain AFGA is not appreciably different from that of the transconductance amplifier, we conclude that the tunneling and injection processes do not contribute significantly to the noise levels.

We want to investigate how changing the AFGA design will change the amount of output noise. Following [10] and [3], we can model the thermal noise component $\hat{i}_o$ of a subthreshold MOSFET's channel current by $\hat{i}_o^2 = (2/\kappa)qU_T g_m \Delta f$. Because the AFGA's output comprises both an nFET and a pFET, the

total thermal-noise current derives from two parallel noise sources. We want to find the output-referred voltage noise, which we obtain from a simplified small-signal circuit. One important simplification is that we can relate $V_{\rm fg}$ to $V_{\rm out}$ by a capacitive divider. We express the signal power of the output-referred voltage noise $\hat{V}_{\rm out}^2$ as

$$\hat{V}_{\rm out}^2 = \left(\frac{C_T}{C_2 g_m}\right)^2 \frac{\hat{i}_o^2}{1+(\omega\tau_h)^2} \tag{27}$$

where τ_h is as defined in Section VI. From this expression, we can calculate the total output-noise power as

$$\hat{V}_{\rm out}^2 = \frac{4}{\kappa}\, qU_T g_m \left(\frac{C_T}{C_2 g_m}\right)^2 \int_0^\infty \frac{1}{1+(\omega\tau_h)^2}\, df \tag{28}$$

which, when we use (17), evaluates to

$$\hat{V}_{\rm out}^2 = \frac{qU_T}{\kappa B}\,\frac{C_T}{C_2 C_o} \tag{29}$$

where the correction term B is as defined earlier. The total output-noise power is roughly proportional to C_w and is inversely proportional to C_L.

Now, we would like to calculate the AFGA dynamic range. We define dynamic range (DR) as the ratio of the maximum possible linear output swing to the total output-noise power. With this definition, which is equivalent to that given in [11], we can express the AFGA dynamic range as

$$\mathrm{DR} = \frac{V_{\rm Lo}^2}{2\hat{V}_{\rm out}^2} = \frac{\kappa}{2q}\, V_{\rm Lo} C_o B^2 \tag{30}$$

which is similar to the form for dynamic range for the wide-linear-range amplifier, as derived in [11]. The dynamic range varies inversely with C_2; therefore, a high-gain amplifier will have a larger dynamic range than will the low-gain amplifier for the same values of C_1, C_w, and C_L.

VII. Conclusions

The AFGA is a simple example of a large class of adaptive floating-gate MOS circuits; these circuits use tunneling and hot-electron injection to adapt the charge on floating gates to return the circuit to a baseline condition on a slow timescale. When the appropriate feedback is applied to the floating gate, this adaptation is an inherent part of the circuit's operation—no additional control circuitry is required. In the case of AFGA, we set up the feedback such that the output voltage returns to its steady-state value on a long timescale. The modulation of the pFET hot-electron injection by the output voltage provides the correct feedback to return the output voltage to the proper operating regime.

The AFGA has four operating regimes. First, in the adaptation regime, the AFGA behaves as a high-pass filter; the timescale is set by the tunneling and injection currents. Second, in the integrating regime, the AFGA behaves as a low-pass filter; the timescale is set by the nFET bias current. Third, for timescales between the adaptation and integrating regimes, the AFGA acts as an amplifier. Fourth, at frequencies much higher than the integrating regime, the AFGA exhibits capacitive feedthrough, which can be reduced by an increase in either C_w or C_L.

The AFGA always is a first-order system, even in the presence of parasitic capacitances; therefore, the AFGA is unconditionally stable, with 90° of phase margin for noninductive loads. An amplifier that has resistive feedback is at least a second-order system, but an amplifier with capacitive feedback can be a first-order system.

MOS devices and quantum processes, such as electron tunneling and hot-electron injection, are often criticized for their high $1/f$ noise. Since the AFGA's noise performance is similar in thermal and $1/f$ characteristics to that of a standard MOS amplifier, the tunneling and injection processes do not add appreciable noise to the amplifier. In addition, with a desired adaptation rate, we can reduce significantly the low-frequency noise generated in the AFGA; such a reduction cannot be obtained in a standard amplifier that has a blocking capacitor at the input. For moderate tunneling currents, the low-frequency time constant can remain nearly constant for timescales measured in years; any shift is due primarily to trapping in the tunneling oxide. We can increase the linear range by increasing C_w, and we can increase the dynamic range by increasing C_w or C_L.

Acknowledgment

The authors thank R. Sarpeshkar for holding several useful discussions and L. Dupre for manuscript editing.

References

[1] E. A. Vittoz, "Dynamic analog techniques," in *Design of MOS VLSI Circuits for Telecommunications*, Y. Tsividis and P. Antognetti, Eds. Englewood Cliffs, NJ: Prentice-Hall, 1985.

[2] P. Hasler, B. A. Minch, C. Diorio, and C. Mead, "An autozeroing amplifier using pFET hot-electron injection," in *Proc. Int. Symp. Circuits and Systems*, vol. 3, Atlanta, GA, 1996, pp. 325–328.

[3] P. Hasler, "Foundations of Learning in Analog VLSI," Ph.D. disseration, California Inst. of Technology, Pasadena, 1997.

[4] Y. Leblebici and S. M. Kang, *Hot Carrier Reliability of MOS VLSI Circuits*. Boston, MA: Kluwer Academic, 1993.

[5] B. A. Minch, C. Diorio, P. Hasler, and C. A. Mead, "Translinear circuits using subthreshold floating-gate MOS transistors," *Analog Integrated Circuits and Signal Processing*, vol. 9, no. 2, pp. 167–179, 1996.

[6] Y. Tsividis, M. Banu, and J. Khaury, "Continuous-time MOSFET-C filters in VLSI," *IEEE Trans. Circuits Syst.*, vol. 33, Feb. 1986.

[7] C. Mead, *Analog VLSI and Neural Systems*. Reading, MA: Addison-Wesley, 1989.

[8] P. Hasler, "Continuous-time feedback in floating-gate MOS circuits," *IEEE Trans. Circuits Syst. II*, vol. 48, pp. 56–64, Jan. 2001.

[9] P. Hasler, C. Diorio, B. A. Minch, and C. Mead, "Single transistor learning synapses," in *Advances in Neural Information Processing Systems 7*. Cambridge, MA: MIT Press, 1995, pp. 817–824.

[10] R. Sarpeshkar, T. Delbruck, and C. A. Mead, "White noise in MOS transistors and resistors," *IEEE Circuits Devices Mag.*, pp. 23–29, Nov. 1993.

[11] R. Sarpeshkar, R. F. Lyon, and C. Mead, "A low-power wide-linear-range transconductance amplifier," *Analog Integr. Circuits Signal Process.*, Nov. 1996.

Paul Hasler (S'87–A'97–M'01) received the B.S.E. and M.S. degrees in electrical engineering from Arizona State University,Tempe, in 1991 and the Ph.D. degree in computation and neural systems from the California Institute of Technology, Pasadena, in 1997.

He is currently an Assistant Professor in the Department of Electrical and Computer Engineering at the Georgia Institute of Technology. His research interests include low-power electronics; mixed-signal integrated circuits and systems; the use of floating-gate MOS transistors to build adaptive information processing systems and "smart" sensor interfaces; the physics of deep submicrometer devices or floating-gate MOS devices; and analog VLSI models of neurobiological learning and sensory information processing.

Dr. Hasler received an NSF Career Award in 2001 and the IEEE Electron Devices Society's Paul Rappaport Award in 1996. He is active in the IEEE as a Cochair of the Atlanta section of the IEEE Electron Devices Society, as a Reviewer for IEEE TRANSACTIONS ON CIRCUITS AND SYSTEMS and IEEE TRANSACTIONS ON NEURAL NETWORKS, and as Cochair for special sessions in the IEEE International Symposium on Circuits and Systems in both 1998 and 1999.

Bradley A. Minch (S'90–M'91) received the B.S. degree in electrical engineering (with distinction) from Cornell University, Ithaca, NY, in 1991 and the Ph.D. degree in computation and neural systems from the California Institute of Technology, Pasadena, in 1997.

He is currently an Assistant Professor in the School of Electrical and Computer Engineering, Cornell University. His research interests include the analog and digital integrated circuit design, translinear circuits, log-domain filters, and adaptive floating-gate MOS circuits.

Dr. Minch is a member of Tau Beta Pi, Eta Kappa Nu, and Phi Kappa Phi. He received the IEEE Electron Devices Society's Paul Rappaport Award in 1996.

Chris Diorio (M'88) received the B.A. degree in physics from Occidental College, Los Angeles, CA, in 1983 and the M.S. and Ph.D. degrees in electrical engineering from the California Institute of Technology, Pasadena, in 1984 and 1997, respectively.

He is presently an Assistant Professor of computer science and engineering at the University of Washington, Seattle. His research focuses on building electronic circuits and systems that mimic the computational and organizational principles found in the nervous systems of living organisms. He has worked as a Senior Staff Engineer at TRW, Inc., as a Senior Staff Scientist at American Systems Corporation, and as a Technical Consultant at The Analytic Sciences Corporation.

Dr. Diorio received an Alfred P. Sloan Foundation Research Fellowship in 2000, a Presidential Early Career Award in Science and Engineering (PECASE) in 1999, a Packard Foundation Fellowship in 1998, an NSF CAREER Award in 1998, and the IEEE Electron Devices Society's Paul Rappaport Award in 1996.